Chain Conformation in Sheared Polymer Melts As Revealed by SANS†

R. Muller,* J. J. Pesce, and C. Picot

Institut Charles Sadron (CRM–EAHP), 4 rue Boussingault, 67000 Strasbourg, France

Received February 8, 1993; Revised Manuscript Received April 21, 1993

ABSTRACT: The conformation of polymer chains in the melt during simple shear flow has been characterized by SANS on a narrow molecular weight distribution polystyrene sample. An apparatus has been designed which allows one to freeze-in by quenching uniform shear orientations in thick specimens on which the scattering experiments can be performed in the three principal shear directions. In the 1–2 shearing plane, the orientation of molecular anisotropy with respect to the shear axes is found to depend on the magnitude of the scattering vector and therefore on the considered length scale on the chain. A method has been proposed to analyze the data in this plane. The chain dimension in the neutral shear direction remains unaffected by the flow. The birefringence and extinction angle have been measured and compared to the SANS data. Finally, the respective influence of shear stress and shear strain on the chain conformation is discussed.

I. Introduction

Small-angle neutron scattering is a very convenient technique for revealing changes in the microscopic chain conformations in a polymeric system under external constraints. For rheological studies of polymer solutions or melts, scattering experiments contribute valuable information about the chain dynamics which, together with macroscopic bulk properties, can help to discriminate between competing molecular models.[1–3]

From an experimental point of view, the scattering measurements can be performed either directly on a sample subjected to deformation or flow during the scattering experiment or on quenched samples where the orientation induced by the flow has been frozen-in. The former technique has been used for rubbers[4,5] and polymer solutions in shear flow,[6,7] whereas the latter is well suited to polymer melts with high glass transition temperatures. Most scattering data which have been obtained in this way for melts concern uniaxially stretched samples[3,8] for which the low thickness of the specimens allows rapid cooling and homogeneous deformation within the samples.

It is the purpose of the present paper to extend the quenching technique to samples deformed in simple shear, which would allow a three-dimensional characterization of the chain conformation with respect to the shear axes by performing the scattering experiments on specimens cut along the three principal shear directions.

Preliminary tests have been carried out on samples sheared in the parallel–plate geometry of a Weissenberg rheogoniometer,[9] but many experimental problems appeared which made the method difficult to use and may even introduce some errors in the scattering data: though the surfaces of the plates were grooved, it was difficult to maintain the adhesion between the polymer and the metallic plates during quenching, due to thermal contraction. Moreover, to minimize the gradient of orientation in the sample thickness resulting from the relaxation during the cooling stage, the gap had to be reduced to 2 mm. Consequently, specimens for SANS experiments where the neutron beam was in the radial direction were very difficult to prepare. Finally, the range of the torque transducer was limited and did not allow shear stresses corresponding roughly to the Newtonian plateau of the polymer melt to be exceeded.

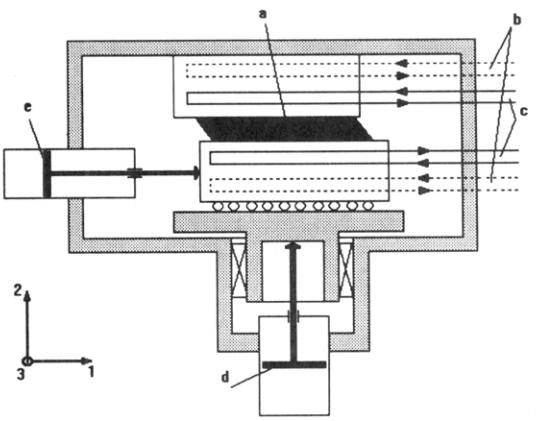

Figure 1. Schematic drawing of the apparatus: (a) specimen; (b) oil circulation; (c) water circulation; (d) normal force jack; (e) shear force jack. 1, 2, and 3 are the principal shear directions.

To overcome these difficulties, a new apparatus has been designed which will be briefly described. In particular, it will be shown how this device allows freezing-in homogeneous orientation in simple shear for samples with a typical thickness of about 5 mm, despite the low thermal conductivity of polymer melts.

The first SANS data on samples sheared with this apparatus were obtained on a narrow molecular weight distribution polystyrene sample, containing labeled deuterated chains with the same molecular weight as the nonlabeled chains. The rheological behavior of this polymer has already been characterized, and scattering data on specimens uniaxially stretched in the melt have been published.[8]

II. Experimental Device and Rheological Results

1. Apparatus. The experimental device constructed to orient the samples in simple shear is schematically represented in Figure 1. It is basically a shear-sandwich type rheometer, the polymer sample being sheared between two temperature-controlled parallel plates with an area of 125 mm × 75 mm and grooved surfaces (depth of the grooves: 0.3 mm). The upper plate is fixed whereas the lower plate can be displaced both horizontally and vertically with two pneumatic jacks.

The shearing experiment occurs in the following way: (a) The temperature of both plates is set to its value during the melt flow by a silicone oil circulation. (b) The polymer sample, which has

† Experiments carried out at the LLB, Laboratoire Commun CEA–CNRS, Saclay, France.

0024-9297/93/2226-4356$04.00/0

been molded in the form of a parallelepiped with typical dimensions 50 mm × 30 mm × 5 mm, is inserted between the plates. (c) During thermal equilibration of the sample, a normal force is applied to the lower plate so that the grooved surface of the plates will penetrate the polymer melt which will keep the sample sticking to the plates during shearing and cooling. This compressive force should be low enough (depending on the melt viscosity) to prevent the sample from being squeezed, which would increase its area. (d) Once thermal equilibration of the sample is achieved, the compressive force is removed from the sample and the gap between the plates is now fixed by a mechanical stop. The orientation which might have been produced by the compression of the sample is allowed to relax by waiting several times the terminal relaxation time of the melt at that temperature before starting the shearing. (e) A constant shear force F is applied to the melt with the horizontal jack during a given time. At the same time, the normal force N in the sample is recorded with a force transducer mounted below the lower plate. From the horizontal displacement measured to a precision of 0.02 mm with an LVDT transducer, the shear strain is obtained as a function of time. (f) After shearing, the sample is cooled by stopping the oil circulation and starting the cold water circulation, which is located close to the surface of the plates. Throughout the cooling stage, both the shear force F and the normal force N are kept constant, the vertical jack being now driven with the same compressive force which has been measured during the shearing stage.

Keeping a constant compressive force on the sample during cooling allows compensation for thermal shrinkage and, with the grooves in the metallic plates, prevents the polymer from slipping away from the surfaces of the rheometer. Furthermore, if the temperature is assumed to be uniform in each polymer layer (at constant height) at any time during cooling (which appears to be justified if the area of the plates is large enough compared to the area of the polymer sample), each polymer layer will experience the same constant shear and normal stresses during quenching. This in turn means that if steady flow is reached at the beginning of the cooling stage (the curves in Figure 2 show that the shear rate becomes constant to within experimental error for shear strains of the order of 1), the orientation will be uniform throughout the whole thickness of the sample, although the inner layers, which will be cooled later, will experience a higher final shear strain than the outer layers in contact with the plates which are quenched first. Birefringence provides an easy way to check the uniformity of orientation in the sample thickness: the observation with a polarizing microscope of small strips cut out vertically in the 1-2 shearing plane (see Figure 4) shows that both the birefringence and the extinction angle (equal to β in Figure 4 if A and B are the principal directions of the polarizability tensor) are uniform throughout the whole thickness.

The same observation also shows that the thickness of the outer layers, where end effects due to the grooved metallic surfaces affect the flow homogeneity, is less than 0.1 mm (these layers have been reamed away on both sides of the sheared polymer plates before cutting the specimens for the SANS experiments). Moreover, the effective thickness of the sheared material to be taken for the calculation of the shear strain from the horizontal displacement of the lower plate of the rheometer is close to the gap between the plates.

2. Sample for the SANS Experiments. The sample used in the present study is a mixture of two anionically synthesized PS samples, one a hydrogenated polymer (PSH) and the second a deuterated polymer (PSD). Both polymers have nearly the same molecular weight distribution: $M_w = 90000$, $M_w/M_n = 1.12$ for PSH and $M_w = 95000$, $M_w/M_n = 1.13$ for PSD. The weight-average polymerization indices are very close for the two polymers: $N = 865$ for PSH and $N = 850$ for PSD. The same sample has already been used in a previous study on chain deformation in uniaxial elongational flow,[8] where details about blending and molding can be found.

3. Typical Stress-Strain Curves. To test the reliability of the shearing procedure, which may be affected by temperature control and end effects at high shear strains (due to the finite ratio of length over thickness of the samples), the shear strain γ has been measured as a function of time for the same shear stress τ_0 and at various temperatures. Since each sample uses about 8 g of polymer, these preliminary tests have been carried out with a commercial PS (Lacqrène 1241H from Elf-Atochem) rather than with the anionic samples containing deuterated chains. According to time-temperature superposition,[10] the various isotherms should superpose according to

$$\gamma(t,T) = \gamma\left(\frac{t}{a_{T\to T_0}},T_0\right) \qquad (1)$$

where $a_{T\to T_0}$ is the thermal shift factor. Figure 2 shows that the $\gamma(t)$ curves at various temperatures can actually be superposed by a shift on the time scale with shift factors close to those determined independently by dynamic viscoelastic measurements. This result indicates a satisfactory control of the temperature and of the kinematics of the flow in the rheometer. The curves in Figure 2 also show that the shear rate (i.e., the slope of the curve $\gamma(t)$) becomes nearly constant for shear strains higher than 1. Thus, the flow becomes steady state from a rheological point of view for relatively moderate strains.

The values of temperature, shear stress, and shear strain which have been chosen for the specimens to be characterized by SANS are summarized in Figure 3, where the dynamic viscosity $\eta^* = (\eta'^2 + \eta''^2)^{1/2}$ has been plotted as a function of the quantity $\omega\eta^*$ at two temperatures. Assuming that the Cox-Merz relation is verified ($\eta^*(\omega) = \eta(\dot\gamma)$ for $\omega = \dot\gamma$) this representation amounts to a plot of the viscosity as a function of shear stress. Changing the temperature shifts this curve only vertically (according to time-temperature equivalence). This means that a given value of the shear stress always corresponds to the same part of the curve (Newtonian plateau or shear-thinning range) and that the temperature only affects the corresponding time scale or shear

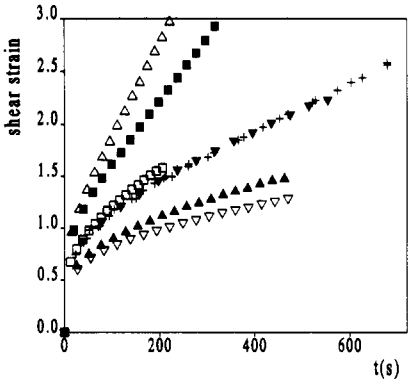

Figure 2. Shear strain as a function of time at various temperatures for the same constant shear stress ($\tau_0 = 10^5$ Pa) on the Lacqrène 1241H sample: 124 (△), 121 (■), 119 (□), 118 (▼), 114 (▲), and 112 °C (▽). Same data shifted according to the reference temperature $T_0 = 118$ °C according to eq 1 (+). The thermal shift factor is $a_{112\to118°C} = 3.3$ between 112 °C and T_0 and $a_{124\to118°C} = 0.26$ between 112 °C and T_0.

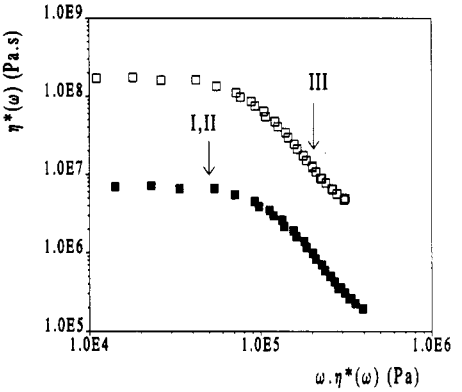

Figure 3. Dynamic viscosity $\eta^*(\omega)$ as a function of $\omega\eta^*(\omega)$ for the PS sample used for the SANS experiments at 120 (□) and 130 °C (■). If the Cox-Merz relation holds, the curves are equivalent to viscosity versus shear stress curves (see text). The arrows indicate the shear flow experienced by samples I, II, and III before quenching ($\tau = 0.05$ MPa and $T = 130$ °C for samples I and II; $\tau = 0.2$ MPa and $T = 120$ °C for sample III).

Table I. Parameters of the Shear Flow, Characteristic Angles of Orientation, and Experimental Mean Square Chain Dimensions in the Various Directions (See Text)[a]

	sample		
	I	II	III
shear stress (Pa)	5×10^4	5×10^4	2×10^5
T (°C)	130	130	120
shear strain	2.8	4	2.4
$\beta_{\Delta n}$ (deg)	64	66	67.5
β_{aff} (deg)	72	76.5	70
β_0 (deg)	~63	~63	71
$R_{g,A}$ (Å)	94	99	143
$R_{g,B}$ (Å)	73	69	47
$R_{g,1}$(exp), 1–3 plane (Å)	89	93	136
$R_{g,3}$(exp), 1–3 plane (Å)	83	83	81
$R_{g,2}$(exp), 2–3 plane (Å)		77	
$R_{g,3}$(exp), 2–3 plane (Å)		83	
$R_{g,1}$(calc) (Å)	91	95	137
$R_{g,2}$(calc) (Å)		75	

[a] Radius of gyration of the isotropic sample: 82 Å.

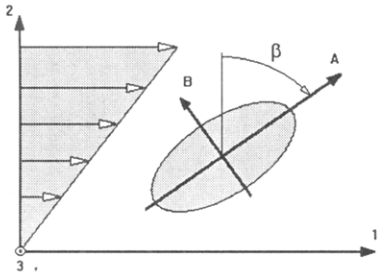

Figure 4. Definition of the principal directions of molecular orientation (A, B) with respect to the principal shear directions (1, 2).

rate. Two values of shear stress have been chosen: one corresponding to the end of the Newtonian plateau (τ = 0.05 MPa) and one corresponding to the shear-thinning behavior of the melt (τ = 0.2 MPa). Time–temperature equivalence allows one to choose the temperature so that the time of the experiment, which for a given shear strain is inversely proportional to the shear rate, remains of the order of a few minutes (T = 120 °C for τ = 0.2 MPa and T = 130 °C for τ = 0.05 MPa). In this way, the time necessary to quench the sample (between 10 and 20 s) remains short compared to the time of the shear flow. For the lowest shear stress, two different samples, corresponding to different shear strains (γ = 2.8 and γ = 4 at the onset of cooling), have been prepared. Table I summarizes the shearing conditions of the three specimens which will be characterized by SANS.

III. Small-Angle Neutron Scattering Results

1. Principal Directions of Orientation. Figure 4 defines the principal directions of molecular anisotropy (A, B, and C) with respect to the principal directions of shear (1, 2, and 3), 1 being the direction of velocity and 2 the normal to the plates. Symmetry of the flow leads to C = 3, and the relative orientation of (A, B) with respect to (1, 2) is defined by the angle β. At vanishing chain orientation (at either small strains or low shear rates) β is expected to be close to 45°, whereas for large affine chain deformation β tends to 90°. More generally, β depends on shear rate or shear stress. It should be emphasized that the value of β depends theoretically on the way the orientation is measured. Birefringence measurements where β is identical to the extinction angle may, for instance, give different values of β than SANS measurements in the range of low scattering vectors (see Table I). This can be qualitatively understood in the framework of molecular models where relaxation mechanisms with different relaxation times are associated with characteristic length scales on the chain.[11] It would be expected that the molecular anisotropy at a local scale on the chain is lower than the anisotropy of the end-to-end vector or radius of gyration. In the particular case of a shear flow, this will result in an orientation with respect to the shear axes which is also depending on the considered length scale; in other words, β in a scattering experiment may depend on the magnitude of the scattering vector.[9]

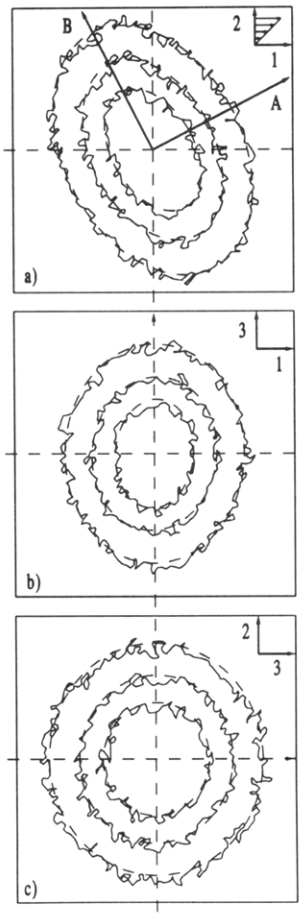

Figure 5. Isointensity curves of sample II in the three principal shearing planes: 1–2 (a); 1–3 (b); (2–3) (c). All isointensity curves are fitted with ellipses. In the 1–2 plane, the minor and major axes define the scattering vectors q_A and q_B, and their orientation with respect to the shear axes defines β. In the 1–3 and 2–3 planes, the axes of the ellipses coincide with the shear axes.

2. SANS Measurements and Analysis of Data. From the sheared and quenched polymer plates, 1-mm-thick specimens were cut in the principal shearing planes: in planes 1–2 and 1–3 for samples I and III and in all three planes (1–2, 1–3, and 2–3) for sample II. The SANS experiments were carried out at the Laboratoire Léon Brillouin, Saclay, France, on a small-angle spectrometer (PAXY) equipped with a two-dimensional multidetector. The range of the scattering vector amplitude was $5.2 \times 10^{-3} < q < 5.5 \times 10^{-2}$ Å^{-1}. Water calibration was used to convert the scattering data to an absolute coherent scattering cross-section, $S(\mathbf{q})$, with units of reciprocal centimeters. The radius of gyration of an isotropic sample was determined from the Zimm plot in the low scattering vector range. The obtained value of 82 Å is in very good agreement with that determined in a previous study on the same sample at the D11 spectrometer of the Institut Laue Langevin in Grenoble.[8]

Figure 5a shows typical isointensity curves on the multidetector for a specimen in the 1–2 shearing plane (for the sake of clarity, only three curves have been plotted). According to the above comments on a possible q dependence of the chain orientation with respect to the shear directions, the scattering data were analyzed as follows:

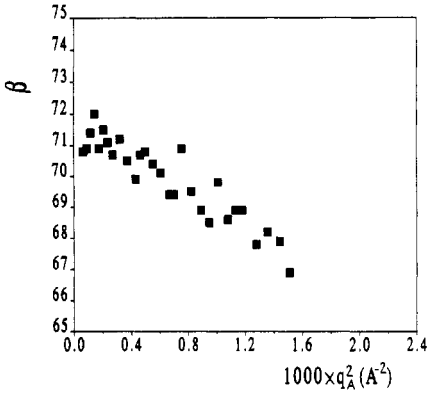

Figure 6. Variation of angle β with the square of the scattering vector in direction A.

each isointensity curve was fitted with an ellipse using a least squares program which determines for each curve both the minor and major axes (which are the scattering vectors q_A and q_B along directions A and B, respectively) and their orientation β with respect to the shear axes. For the data of the present study, the shape of all isointensity curves was almost elliptical, so that the fit was possible to a good approximation (see Figures 5a and 8).

Figure 6 shows the variation of β as a function of the minor axis q_A for the isointensity curves of sample III. Despite some scatter in the data (which could be reduced by increasing the time of measurement), it appears that for low q values (typically $q_A < 2.5 \times 10^{-2}$ Å^{-1}, which corresponds to $q_B < 5.5 \times 10^{-2}$ Å^{-1}) β levels off to a value β_0 of the order of 71°. This angle can be compared on the one hand to the extinction angle $\beta_{\Delta n}$ of birefringence and on the other hand to the orientation β_{aff} of the principal directions of the Cauchy deformation tensor, which would correspond to a molecular deformation purely affine with the macroscopic deformation shear strain. For a simple shear deformation γ, the Cauchy deformation tensor is given by

$$\underline{\underline{B}} = \begin{pmatrix} 1+\gamma^2 & \gamma & 0 \\ \gamma & 1 & 0 \\ 0 & 0 & \end{pmatrix} \tag{2}$$

Hence

$$\beta_{\text{aff}} = \frac{1}{2}\arctan\left(-\frac{2}{\gamma}\right) \tag{3}$$

It appears that for sample III the value of β_0 determined from the SANS isointensity curves in the low q range is higher than $\beta_{\Delta n}$ and close to β_{aff} (see Table I). Furthermore, Figure 6 clearly shows that β decreases with increasing magnitude of the scattering vector, thus confirming the idea that the direction of molecular orientation in shear flow depends on the considered length scale on the chain: the overall chain orientation is closer to that of an affine deformation than the local chain orientation.[9] The extinction angle of birefringence should then represent some average of β over the whole q range. Since for the highest q value of the present set of experiments β is roughly equal to $\beta_{\Delta n}$ (see Figure 6), this should be confirmed by complementary measurements in a higher q range, where it is expected that β will take values below $\beta_{\Delta n}$.

The same analysis has been carried out for samples I and II at lower shear stresses. As can be seen in Figure 8, the anisotropy of the isointensity curves was lower for these samples, with the consequence that the error on the determination of β was significantly higher (of the order ±3° instead of ±1° for sample III). The average of β was around 63° for both samples I and II with no clear q dependence, due to increased scatter on the data. It can nevertheless be noticed that the β values determined from SANS data for samples I and II are (a) close to each other and lower than for sample III and (b) closer to $\beta_{\Delta n}$ than to β_{aff} (see Table I).

For all three samples, it can be assumed that β becomes independent of q in the low q range ($\beta = \beta_0$). As a consequence, one can determine a mean square dimension of the chain in the direction of β_0 and in the perpendicular direction $\beta_0 + \pi/2$ from a Zimm plot of the scattered intensity as a function of q_A and q_B, respectively. More precisely, the form factor in the Guinier range can be written as[12]

$$g(q) = N\left(1 - \left\{q_A^2\frac{\sum_{n,m}\langle x_{A,nm}^2\rangle}{2N^2} + q_B^2\frac{\sum_{n,m}\langle x_{B,nm}^2\rangle}{2N^2} + q_C^2\frac{\sum_{n,m}\langle x_{C,nm}^2\rangle}{2N^2}\right\}\right) = N(1 - \{q_A^2X_A^2 + q_B^2X_B^2 + q_C^2X_C^2\}) \tag{4}$$

where N is the number of scattering units per chain and $x_{A,nm}$, $x_{B,nm}$ and $x_{C,nm}$ are the coordinates in three perpendicular directions of the position vector between two scattering units n and m. In this expression, X_A^2, X_B^2, and X_C^2 represent the mean square distance between scattering units in the directions A, B, and C, respectively. For the particular case of an isotropic distribution, $X_A^2 = X_B^2 = X_C^2$, and

$$g(q) = N\left(1 - q^2\frac{R_g^2}{3}\right) \tag{5}$$

where $R_g = (X_A^2 + X_B^2 + X_C^2)^{1/2}$ is the radius of gyration. Anisotropic systems are analyzed with the scattering vector along various directions (A, B, and C). For the sake of comparison, characteristic mean square dimensions $R_{g,A}$, $R_{g,B}$, and $R_{g,C}$ in these directions are introduced which reduce to the radius of gyration in the isotropic case: $R_{g,A}^2 = 3X_A^2$, $R_{g,B}^2 = 3X_B^2$, $R_{g,C}^2 = 3X_C^2$. A relation similar to eq 5 then holds in each direction. For instance, in the A direction

$$g(q_A) = N\left(1 - q_A^2\frac{R_{g,A}^2}{3}\right) \quad \text{or} \quad g^{-1}(q_A) = \frac{1}{N}\left(1 + q_A^2\frac{R_{g,A}^2}{3}\right) \tag{6}$$

since in the Guinier range $qR_g \ll 1$. Figure 7 shows as an example the Zimm plot of sample III obtained by plotting (for each isointensity curve in the 1–2 shearing plane) the inverse of the normalized scattering intensity as a function of q_A^2 and q_B^2 (q_A and q_B being the minor and major axes of the ellipse fitted to that isointensity curve). By comparing Figures 7 and 6, it appears that in the low q range where the Zimm plots become linear ($q_A^2 < 5 \times 10^{-4}$ Å^{-2} or $q_B^2 < 2.5 \times 10^{-3}$ Å^{-2}) β can also be considered as q-independent, which means that $R_{g,A}$ and $R_{g,B}$ determined from the initial slopes according to eq 6 actually represent a mean square chain dimension in the directions β_0 and $\beta_0+\pi/2$. The data for $R_{g,A}$ and $R_{g,B}$ for the three samples are given in Table I.

From specimens cut in the 1–3 and 2–3 shearing planes, mean square chain dimensions similar to $R_{g,A}$ and $R_{g,B}$ can also be determined in the principal shear directions 1, 2,

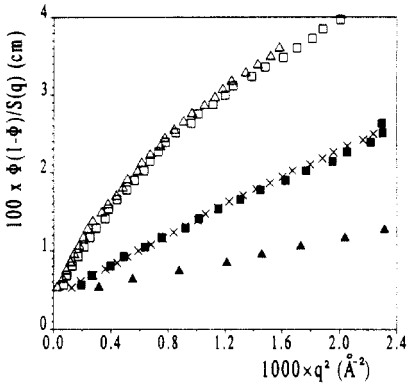

Figure 7. Zimm plot of the absolute coherent scattering cross-section reduced to the concentration of deuterated species for sample II: in the direction of q_A (△) and of q_B (▲) and in the directions 1 (□) and 3 (■) compared to the isotropic sample (×). The curves extrapolated at zero q are found to intersect the y-axis at the same value. From their initial slope, one can calculate $R_{g,A}$, $R_{g,B}$, $R_{g,1}$, and $R_{g,3}$.

and 3. Typical isointensity patterns in the three shearing planes are shown in Figure 5 for sample II. It can be seen that the shape of these curves in the 1–3 and 2–3 planes is nearly elliptical like in the 1–2 plane. However, due to the symmetry of the shear flow, the 3 direction is a principal direction for molecular orientation at all scales, and the major and minor axes of the isointensity curves are indeed found to be parallel to the {1,3} and {2,3} directions. Therefore, the analysis of the scattering data in the 1–3 and 2–3 planes has been carried out by fixing the direction of the axes of the ellipse (to 0° and 90°) in the least-squares fit program. The major and minor axes of these ellipses then define the scattering vectors q_1, q_2, and q_3 in the principal shear directions and allow calculation of the mean square chain dimensions $R_{g,1}$, $R_{g,2}$, and $R_{g,3}$ (see Figure 7).

3. Relationships between the Mean Square Chain Dimensions in the Different Directions. Obviously, $R_{g,A}$ and $R_{g,B}$ are not independent of $R_{g,1}$ and $R_{g,2}$. From the relations between x_1, x_2 and x_A, x_B

$$x_1 = x_A \sin\beta_0 - x_B \cos\beta_0$$

$$x_2 = x_A \cos\beta_0 + x_B \sin\beta_0 \qquad (7)$$

the following relations between the mean square coordinates are obtained:

$$\langle x_1^2\rangle = \langle x_A^2\rangle \sin^2\beta_0 + \langle x_B^2\rangle \cos^2\beta_0 - 2\langle x_A x_B\rangle \sin\beta_0 \cos\beta_0$$

$$\langle x_2^2\rangle = \langle x_A^2\rangle \cos^2\beta_0 + \langle x_B^2\rangle \sin^2 B_0 + 2\langle x_A x_B\rangle \sin\beta_0 \cos\beta_0 \qquad (8)$$

If the principal directions for the chain orientation were β_0 and $\beta_0+\pi/2$ at all scales, the mean value of the product $x_A x_B$ would be zero (due to the symmetry of the conformation distribution with respect to the A and B axes). In this case, the following relations between the mean square chain dimensions would hold:

$$R_{g,1}^2 = R_{g,A}^2 \sin^2\beta_0 + R_{g,B}^2 \cos^2\beta_0$$

$$R_{g,2}^2 = R_{g,A}^2 \cos^2\beta_0 + R_{g,B}^2 \sin^2\beta_0 \qquad (9)$$

In Table I, the experimental values of $R_{g,1}$ and $R_{g,2}$ determined in the 1–3 and 2–3 shearing planes are compared to the values calculated from $R_{g,A}$, $R_{g,B}$, and β_0 according to eq 9. The observed agreement indicates that the q dependence of β at local scales as shown in Figure 6 has little influence on the mean square chain dimensions $R_{g,A}$ and $R_{g,B}$. As a matter of fact, these quantities are determined in the low q range and involve mainly large-scale position correlations for which the principal directions of orientation are indeed equal to β_0 and $\beta_0+\pi/2$.

Another interesting result is obtained from the comparison of the scattering of the sheared samples in the 3 direction to that of an isotropic sample. Figure 7 shows the Zimm plot of sample III in the directions 1 and 3 for a specimen cut in the 1–3 plane. The corresponding curve for an isotropic sample, which has also been plotted in the same figure, is found to be identical to within experimental error to the curve in the 3 direction. This result indicates that the position correlations within the chain in the neutral direction of the shear flow are not affected by the flow, at least up to the values of stress and strain used in the present study. In particular, Table I shows that the mean square chain dimension in that direction, $R_{g,3}$, which has been determined either in the 1–3 or in the 2–3 planes for the various samples, is found to be equal to the radius of gyration of an isotropic sample to within experimental error ($R_{g,3} = 82 \pm 1$ Å). The same result has been found by Lindner in dilute solutions.[13]

IV. Discussion

1. Influence of Shear Stress and Shear Strain on the Chain Conformation. At a stress level of 0.05 MPa (samples I and II), the creep curves $\gamma(t)$ become linear to within experimental error after a time roughly equal to the terminal relaxation time of the polymer melt at the temperature of the flow, which corresponds to a shear strain of the order of 1. Although the flow appears to be steady state from a rheological point of view, the data in Table I show that the mean square chain dimensions $R_{g,A}$ and $R_{g,B}$ still slightly increase between $\gamma = 2.8$ and $\gamma = 4$, whereas the direction β_0 of the overall orientation of the chains seems to level off to a constant value. Even if the differences between the scattering data of samples I and II are not very pronounced (see Figure 8), it turns out that the chain conformation as characterized by SANS in the low q range is more sensitive than the creep behavior to determine if a steady flow is really attained.

The influence of shear stress at a given shear strain is visualized in Figure 8 by comparing the data of samples I and III and is found to be very pronounced both on the chain anisotropy and on the principal directions of orientation. For sample III, the creep curve appears to be steady state for about the same value of the shear strain ($\gamma \cong 1$) as for samples I and II. But here, this level of strain is reached after a time which is 1 order of magnitude below the terminal relaxation time of the melt at the temperature of the flow (120 °C). SANS data at various strains for that value of stress would certainly be helpful to better understand this result.

2. Calculation of $\beta_{\Delta n}$ from a Giesekus-Type Constitutive Equation. As can be seen in Figure 3, the shear stress for samples I and II has been chosen low enough so that the viscosity of the melt is very close to the zero-shear viscosity at that temperature. Therefore, it could have been expected that the principal directions of orientation remain close to that of a Newtonian liquid (i.e., $\beta \cong 45°$). However, the experimental values of both β_0 and $\beta_{\Delta n}$ are much higher. To clarify this point, the extinction angle of birefringence has been calculated from a constitutive equation by assuming that the stress-optical law is linear.[14]

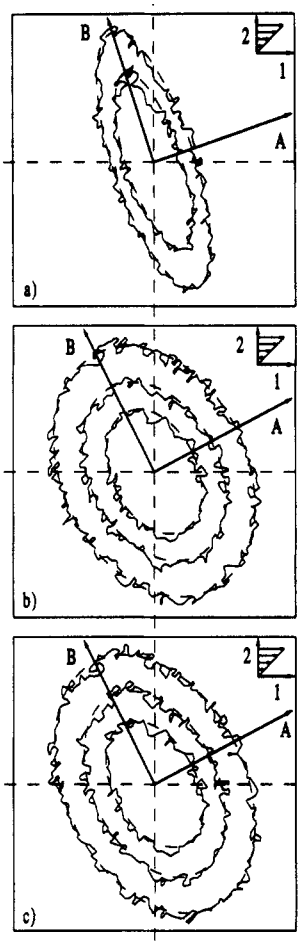

Figure 8. Isointensity curves in the 1–2 shearing plane of the three samples.

For a discrete relaxation spectrum (G_i, λ_i), the Giesekus constitutive equation can be written[15,16]

$$\lambda_i \overset{=}{\frac{\delta \tau_i}{\delta t}} + \underset{=}{\tau_i} + \frac{\alpha}{G_i} \underset{=}{\tau_i} \cdot \underset{=}{\tau_i} = 2G_i \lambda_i \underset{=}{D}$$

$$\underset{=}{\tau} = \sum_i \underset{=}{\tau_i} \tag{10}$$

where δ/δ_t is the upper convected time derivative, $\underset{=}{D}$ is the strain rate tensor, and α is an adjustable parameter. The value of α which gives the best agreement for the viscosity data is close to 0.5 (see Figure 9). A relaxation spectrum with $n = 13$ relaxation times (two per decade) has been determined by adjusting the experimental G' and G'' master curves at 130 °C.[8] The n differential equations have then been solved for a steady shear flow at a given shear rate. After summation of the $\underset{=}{\tau_i}$ in the different modes the principal directions of $\underset{=}{\tau}$ can be calculated. The corresponding angle β (which is also the extinction angle of birefringence for linear stress-optical behavior) and the steady-state shear viscosity have been plotted as a function of shear stress in Figure 9. The experimental data of Figure 3 for the dynamic viscosity at 130 °C have also been reported and show that the Giesekus model satisfactorily describes the shear-thinning behavior of the melt. On the other hand, the value of β calculated for a shear stress of 0.05 MPa is close to 57°, which is below the experimental values around 65°. It is nevertheless interesting to notice that the values of β calculated from the model rapidly increase above 45° in a range of shear stresses where the viscosity is still very close to its low-shear limiting value.

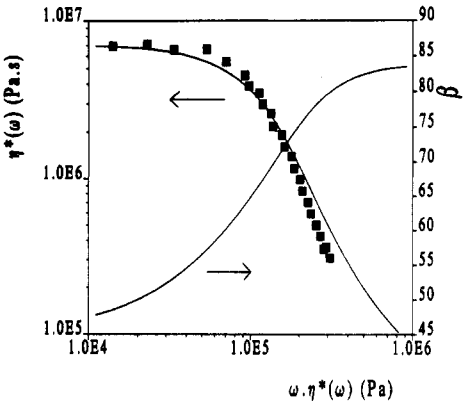

Figure 9. Data at 130 °C of Figure 3 (■) compared to the steady shear viscosity calculated as a function of shear rate (full line) according to the Giesekus model (see text). Orientation angle with respect to the shear axes of the principal directions of the stress tensor calculated with the same model in steady shear flow.

At least qualitatively, this result is in agreement with our SANS data on samples I and II.

3. Estimation of $R_{g,A}$ and $R_{g,B}$ from a Simple Network-Type Calculation. In a previous paper on uniaxial chain deformation, we proposed a simple model to calculate the anisotropic form factor of the chains in a uniaxially deformed polymer melt.[8] The only parameters are the deformation ratio λ of the entanglement network (which was assumed in ref 8 to be identical to the macroscopic recoverable strain) and the number n_e of entanglements per chain. For a chain with dangling end submolecules[17] the mean square dimension in a principal direction of orientation can be written

$$R_g^2(\lambda) = R_{g,iso}^2 \left[1 + (\lambda^2 - 1)\left(1 - \frac{1}{n_e} - \frac{7}{2n_e^2} + \frac{3}{n_e^3} \right) \right] \tag{11}$$

where λ is the network deformation ratio in that direction. The number of entanglements per chain is given to a first approximation by

$$n_e \cong \frac{M G_N^0}{\rho R T} \tag{12}$$

where M is the molecular weight of the chain and G_N^0 is the plateau modulus. For the sample of the present study we get from eq 12 $n_e \cong 5$. A molecular deformation ratio λ in the directions A and B can be estimated in the following way: the difference $\Delta\sigma$ between the principal stresses in the 1–2 plane can be readily calculated from the birefringence Δn (measured parallel and perpendicular to the direction of extinction) and the stress–optical coefficient C for molten polystyrene[18] ($C = 4.8 \times 10^{-9}$ Pa^{-1}):

$$\Delta\sigma = \Delta n / C \tag{13}$$

According to the classical network theory, the stress tensor is proportional to the Cauchy deformation tensor, which means that the network deformation along the principal directions of the stress tensor are λ and $1/\lambda$, where

$$\lambda^2 - \frac{1}{\lambda^2} = \frac{\Delta\sigma}{G_N^0} \tag{14}$$

The values of λ calculated from eq 14 are given in Table II. It should be pointed out that the classical rubber theory does not of course account for a dependence of molecular orientation on the considered length scale, as found for sample III in Figure 6. Therefore the simplistic approach presented here should in principle be restricted to samples I and II for which the principal directions for the low-q

Table II. Extension Ratio and Mean Square Dimensions in the Principal Directions of Stress Calculated from the Network Model (See Text)

	sample		
	I	II	III
Δn	9.4×10^{-4}	1.08×10^{-3}	3.8×10^{-3}
$\beta_{\Delta n}$ (deg)	64	66	67.5
$\Delta\sigma$ (Pa)	2×10^5	2.3×10^5	8.1×10^5
λ	1.27	1.32	2.07
$1/\lambda$	0.79	0.76	0.48
$R_g^2(\lambda)$ (Å)	98	101	148
$R_g^2(1/\lambda)$ (Å)	70	69	56
$R_{g,A}$ (Å)	94	99	143
$R_{g,B}$ (Å)	73	69	47

SANS data (A and B) are close to the principal directions for the refractive index. The data in Table II actually show a satisfactory agreement between calculated and experimental mean square chain dimensions for samples I and II. For sample III, the agreement is less satisfactory in the direction perpendicular to the chain elongation, but one must be aware that for this sample the directions in which $R_{g,A}$ and $R_{g,B}$ have been measured are different from those corresponding to the calculation of eq 14.

V. Conclusion

One of the objectives of the present study was to improve the preparation of sheared specimens for a complete characterization of the chain conformation by SANS measurements with the scattering vector in the three principal shearing planes. The apparatus which has been specifically designed for this purpose actually allows one to quench thick specimens with homogeneous orientation in simple shear throughout the thickness.

The data obtained with the scattering vector in the 1–2 shearing plane confirmed that the principal directions of orientation depend on the magnitude of the scattering vector and therefore on the considered length scale on the chain. On the other hand, the position correlations within the chain in the neutral direction of the flow have been found to remain unaffected by the shear deformation.

An important result was the good correlation between the mean square chain dimensions determined in the different shearing planes, which confirms the reliability of the SANS experiments. Sections IV.2 and IV.3 illustrate how SANS data in simple shear can be used to discuss the validity of rheological models, but it also appeared how important it was for such data to have good statistics for the scattering, which means increased counting time. Further experiments will be necessary to analyze the time evolution of the chain conformation during a creep test at high shear stress.

Acknowledgment. Technical assistance provided by Dr. A. Brûlet and Dr. F. Boué during the SANS experiments at the LLB is gratefully acknowledged.

References and Notes

(1) Boué, F. *Adv. Polym. Sci.* **1987**, *82*, 47.
(2) Boué, F.; Bastide, J.; Buzier, M.; Collette, C.; Lapp, A.; Herz, J. *Prog. Colloid Polym. Sci.* **1987**, *75*, 152.
(3) Bastide, J.; Buzier, M.; Boué, F. *Springer Proc. Phys.* **1987**, *29*, 112.
(4) Boué, F.; Bastide, J.; Buzier, M. *Springer Proc. Phys.* **1988**, *42*, 65.
(5) Picot, C. *Prog. Colloid Polym. Sci.* **1987**, *75*, 83.
(6) Lindner, P.; Oberthür, R. *Colloid Polym. Sci.* **1985**, *263*, 443.
(7) Lindner, P.; Oberthür, R. *Physica B* **1989**, *156*, 410.
(8) Muller, R.; PIcot, C.; Zang, Y. H.; Froelich, D. *Macromolecules* **1990**, *23*, 2577.
(9) Muller, R.; Picot, C. *Makromol. Chem., Macromol. Symp.* **1992**, *56*, 107.
(10) Ferry, J. D. *Viscoelastic Properties of Polymers*, 3rd ed.; John Wiley & Sons: New York, 1980.
(11) Doi, M.; Edwards, S. F. *The Theory of Polymer Dynamics*; Oxford University Press: Oxford, 1986.
(12) Guinier, A.; Fournet, G. *Small Angle Scattering of X-rays*; John Wiley & Sons: New York, 1955.
(13) Lindner, P. *Neutron, X-Ray and Light Scattering*; Lindner, P., Zemb, T., Eds.; North-Holland: Amsterdam, 1991.
(14) Janeschitz-Kriegl, H. *Polymer Melt Rheology and Flow Birefringence*; Springer-Verlag: Berlin, 1983.
(15) Giesekus, H. *Rheol. Acta* **1966**, *5*, 29.
(16) Larson, R. G. *Constitutive Equations for Polymer Melts and Solutions*; Butterworths: Boston, 1988.
(17) Ullman, R. *Macromolecules* **1982**, *15*, 1395.
(18) Muller, R.; Froelich, D. *Polymer* **1985**, *26*, 1477.